


An investigation of artificial neural network structure and its effects on the estimation of the low-cycle fatigue parameters of various steels

Mehmet Alperen Soyer¹ | Nail Tüzün¹ | Özler Karakaş¹ | Filippo Berto² 

¹Department of Mechanical Engineering,
Faculty of Engineering, Pamukkale
University, Denizli, Turkey

²Department of Chemical Engineering
Materials Environment, Sapienza
University of Rome, Rome, Italy

Correspondence

Özler Karakaş, Department of Mechanical
Engineering, Faculty of Engineering,
Pamukkale University, 20160 Denizli,
Turkey.
Email: okarakas@pau.edu.tr

Abstract

Artificial neural networks (ANNs) are a widely used machine learning approach for estimating low-cycle fatigue parameters. ANN structure has its parameters such as hidden layers, hidden neurons, activation functions, training functions, and so forth, and these parameters have a significant influence over the results. Three hidden layer combinations, the hidden neurons ranging from 1 to 25, and different activation functions like hyperbolic tangent sigmoid (tansig), logistic sigmoid (logsig), and linear (purelin) were used, and their effects on the low-cycle fatigue parameter estimation were investigated to determine optimal ANN structure. Based on the results, suggestions regarding ANN structure for the estimation of the low-cycle fatigue parameters and transition fatigue life were presented. For the output layer and hidden layers, the most suitable activation function was tansig. The optimal hidden neuron range has been found between 4 and 9. The neural network structure with one hidden layer was determined to be most suitable in terms of less knowledge, structural complexity, and computational time and power.

KEYWORDS

artificial neural networks, artificial neural network structure, low-cycle fatigue, low-cycle fatigue parameters, transition fatigue life

1 | INTRODUCTION

Artificial neural networks (ANNs) usually consist of highly complex network structures. However, this enables ANNs to solve any type of problem by optimizing their structure. ANNs generally have three layers: input, hidden, and output. Inputs, outputs, and hidden layer (HL) numbers can be customized according to the problem. Some problems require many inputs to solve the problem. For many researchers,^{1–5} increasing the HL

has the advantage of performance and estimation accuracy increase over single-layer perceptron. On the other hand, increasing the number of HLs often led to structural complexity, which slowed the estimation process and occasionally caused overfitting problems. For this reason, increasing the inputs and HLs is not always recommended. In addition, small datasets do not require structural complexity to solve the problem while larger datasets may require complex and well-optimized structures. Generally, the users can start with simple

This is an open access article under the terms of the [Creative Commons Attribution-NonCommercial-NoDerivs](https://creativecommons.org/licenses/by-nc-nd/4.0/) License, which permits use and distribution in any medium, provided the original work is properly cited, the use is non-commercial and no modifications or adaptations are made.

© 2023 The Authors. *Fatigue & Fracture of Engineering Materials & Structures* published by John Wiley & Sons Ltd.

structures to estimate the outputs and increase the complexity of the structure if it is deemed to be inadequate to solve the problem. A simple ANN structure has only one HL. On the other hand, an ANN structure with multiple HLs is called a multilayer perceptron (MLP) or deep neural network (DNN). The input and output layers should not be counted as the HLs. There are a lot of hyperparameters such as training functions, activation functions, hidden neuron numbers, epoch numbers, HL numbers, training ratios, testing ratios, and validation ratios. All these parameters must be selected properly because these hyperparameters are significantly affecting results such as training, testing, validation regressions, and errors. ANNs require high computational power and memory; for this reason, the elapsed time must be considered while estimating the outputs. All the parameters mentioned above also have a significant impact over the elapsed time. The main goal should be to lower the elapsed time and error rates while increasing the estimation accuracy. Optimization of these parameters is especially important for obtaining low-cycle fatigue (LCF) parameters since conventional fatigue testing is a costly and time-consuming process. However, it must be emphasized that fatigue assessments are crucial for structural durability evaluations. Training a neural network to estimate LCF parameters can aid these conventional fatigue estimation methods, potentially lowering costs associated with fatigue testing. However, it is not practical for users to optimize the ANN structure for each fatigue assessment. The aim of this paper is to serve as a potential network structure recommendation for interested parties who would like to use ANN to estimate fatigue parameters and transition fatigue life.

A brief investigation of the state of the art regarding ANN structures and fatigue assessments using ANN reveals the rising popularity of neural networks in fatigue estimations. Soyer et al.⁶ estimated high-strength steel's LCF parameters and fatigue life using ANNs with one HL. The used dataset consisted of 38 high-strength steel, which is a small dataset. They also recommended that 5–20 is adequate for estimating the LCF parameters with small datasets. The LCF parameters and fatigue life estimation accuracy were over 99.99%. As mentioned above, small datasets do not require structural complexity in estimation problems. Hojjat⁷ predicted accurately the Nusselt number of non-Newtonian nanofluids with the ANN approach and used particle swarm optimization for training. ANN structure consisted of two HLs with six and nine neurons, respectively; the activation functions in the HLs were hyperbolic tangent sigmoid (tansig), and the output's activation function was linear (purelin). Raghu and Sriraam⁸ worked on the optimal configuration of the MLP classifier. They used tansig, logistic

sigmoid (logsig), purelin, and Elliot symmetric sigmoid (elliotsig) activation functions. They concluded that linear activation function was more suitable for the output layer than the HLs and tansig was more suitable for the HLs. Also, they tested six different training functions, and the best training function was Levenberg–Marquardt (trainlm) among all. Zadeh et al.⁹ predicted daily outflow by MLP using two HLs. They compared two combinations of activation functions: tansig–tansig–purelin and logsig–logsig–purelin in HL1–HL2–output layer and four to six hidden neurons, respectively. They showed that tansig performed better than the logsig in HLs. Altikat¹⁰ predicted CO₂ emissions with DNN using two HLs with trainlm training function and logsig activation function in the HLs. Altikat tested different combinations of hidden neurons in each HL, and the lowest MAE for the two HL combinations was 14–10 neurons, respectively. Karsoliya¹¹ explained that unnecessarily increasing the HLs brings structural complexity and high amounts of time. In addition, even if the main goal is high estimation accuracy, increasing the HL numbers up to three was considered enough. There is no need to increase the HL number by more than four due to time, complexity, and overfitting issues. Usually, one or two HLs are sufficient for nonlinear estimation problems. In addition, Shen et al.¹² studied neural network approximation, and they concluded that three HLs are sufficient for estimation with high accuracy. Pareek et al.¹ highlighted that the universal approximation theory proposes that one HL with large enough hidden neurons can handle any prediction problem. Collins and Tissot² used one HL to predict thunderstorms with ANN and remarked that one HL is sufficient for the prediction. Al-kaf et al.³ predicted diesel fuel properties with the ANN approach and compared single-layer and multilayer performance. They concluded that a single layer achieved better estimation accuracy than complex methodologies. Uzair and Jamil⁴ investigated the effects of HLs on the efficiency of neural networks. In line with previously mentioned inferences, they concluded that a large number of HLs significantly slow the training process. Increasing the HLs provides better accuracy, but if the time complexity is the main goal, then lowering the HLs was deemed as the better solution, also pointing out the overfitting issues of highly complex network structures. Additionally, Tran et al.⁵ demonstrated that the single layer performed better than the two and three HLs. They remarked that increasing the HL number beyond a certain point led to structural complexity, which slows the training process without significantly improving the performance. Therefore, four and more HL numbers are not considered in this study. Increasing the hidden neuron numbers in one HL structure causes a significant

increase in time, and it increases exponentially by adding more layers.

In addition, there are various algorithms for predicting different types of materials manufactured by different fabrication methods. Kalayci et al.¹³ estimated fatigue lives of magnesium alloy welds by means of bee colony intelligence. The model showed good agreement to fit the Wöhler lines with high accuracy. Karakas et al.¹⁴ estimated the fatigue strength of welded joints in

magnesium alloy using genetic algorithm. They estimated the fatigue strength in heat affected zone with 0.8% and 0.6% for the weld metal. Zhou et al.¹⁵ estimated the fatigue life of friction stir welded aluminum alloys with the ANN/genetic hybrid algorithm. They also noted that the ANN/genetic hybrid algorithm is superior to ANN in terms of predicting fatigue properties. Zeng et al.¹⁶ estimated the fatigue properties of stainless steel fabricated with selective laser melting and S-N

TABLE 1 Research with different numbers of hidden layer numbers and activation functions.

Hidden layer 1	Hidden layer 2	Hidden layer 3	Hidden layer 4	Output layer	Used hidden layer number	Reference
Logsig	Logsig	Logsig	Logsig	Logsig	4 hidden layers	20
Tansig	Tansig	Tansig	-	Tansig	3 hidden layers	21
Logsig	Logsig	Logsig	-	Purelin	3 hidden layers	22
Tansig	Tansig	-	-	Purelin	2 hidden layers	7
Tansig	Tansig	-	-	Purelin	2 hidden layers	23
Tansig	Tansig	-	-	Purelin	2 hidden layers	24
Logsig	Logsig	-	-	Purelin	2 hidden layers	25
Tansig	-	-	-	Purelin	1 hidden layer	26
Tansig	-	-	-	Purelin	1 hidden layer	27
Tansig	-	-	-	Purelin	1 hidden layer	8
Tansig	-	-	-	Tansig	1 hidden layer	28
Tansig	-	-	-	Purelin	1 hidden layer	29
Logsig	-	-	-	Logsig	1 hidden layer	6
Logsig	-	-	-	Logsig	1 hidden layer	30
Logsig	-	-	-	Logsig	1 hidden layer	31
Logsig	-	-	-	Logsig	1 hidden layer	32
Logsig	-	-	-	Purelin	1 hidden layer	33

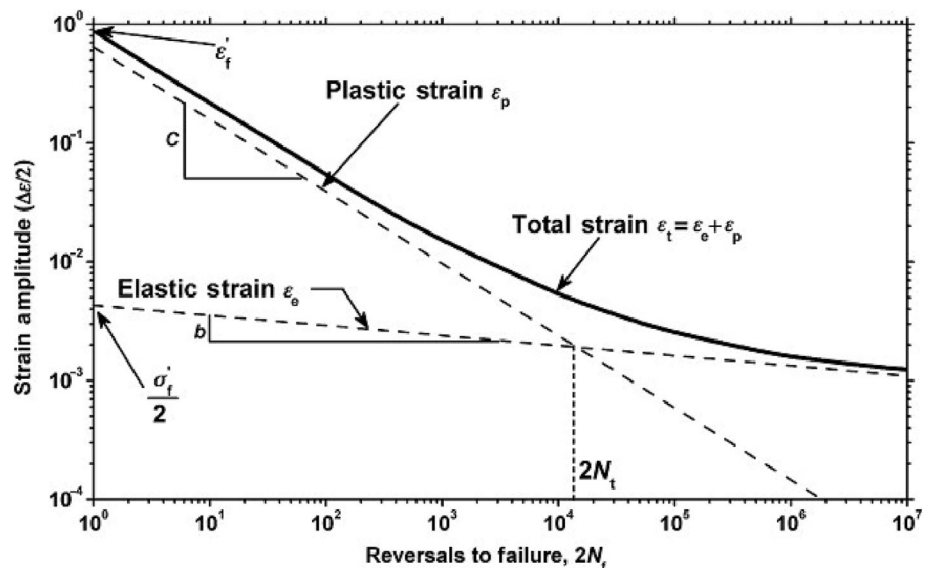


FIGURE 1 Strain amplitude and reversals to failure curve.⁴⁵

curve via dynamic multiswarm particle optimization successfully. Moghaddam et al.¹⁷ predicted the fatigue life of polyethylene terephthalate-modified asphalt mixtures with the support vector machine firefly algorithm. They also compared the algorithm with the support vector machine, genetic algorithm, and ANN in terms of predicting the fatigue life. Also, Karakas et al.¹⁸ mentioned the importance of the data science and machine learning methodologies for fatigue and fracture assessment to overcome various difficulties like time, knowledge, and cost with various published studies in the virtual special issue.

Table 1 shows various research about the estimation of fatigue properties with different activation functions and HL numbers. Only the output layer's activation function has been changed by the researchers. The activation function combinations in more than two HLs are the same as the first HL. The most widely used output activation function was purelin, and the most used activation function in HLs was equally tansig and logsig. In addition, the reason purelin is never used in HLs is if all activation functions of the layers including the output are purelin, then there is no importance in using more than one HL because the last activation function of the output layer becomes a linear function of the first layer's input.¹⁹ Also, the purelin activation function provides better correlation coefficients in the output layer.

As stated before, the estimation of the LCF parameters is vital for safety, cost, and time considerations. Obtaining the LCF parameters by means of conventional methods is a costly and time-consuming process. To lower the time and cost, machine learning approaches can be adapted. The ANN is the overwhelmingly popular and widely used approach for estimating the fatigue life of materials.³⁴ The LCF parameters,^{6,30,35,36} fatigue

lives,^{28,37–39} cyclic properties,^{40,41} and stress–strain curves^{42,43} have been estimated in various research.

Fatigue damage is an unpredictable phenomenon and is very difficult to detect before a sudden failure occurs. High stress amplitude and low frequency often cause fatigue damage to accumulate faster in comparison to low stress amplitude with high frequency, thereby lowering the fatigue lives of components. Due to the rapid deterioration of structural stability, LCF is usually considered more dangerous than high-cycle fatigue (HCF). In LCF, the number of cycles to failure is less than the 5×10^4 cycles, and the main deformation is plastic; thus, the deformation is irreversible. As the load cycle repeats, the deformation continues to accumulate until fatigue failure occurs. Since most work conditions require components to endure loads high enough to cause fatigue damage, estimation of fatigue lives is essential to eliminate the risk of sudden and unexpected failures. For this reason, the present study estimates the fatigue lives

TABLE 2 A summary of the ANN structure parameters.

Hidden layer number	1–3
Hidden neuron range	1–25
Activation functions	Tansig, logsig, purelin
Training function	Levenberg–Marquardt
Inputs	E , RA%, BHN, σ_y , σ_u
Outputs	b , c , $\sigma'f$, $\epsilon'f$, N_f
Dataset size	73
Data division	75% training, 25% testing
Error type	Mean squared error (MSE)
Maximum epoch	100
Normalization process	mapminmax
Software	MATLAB R2022a

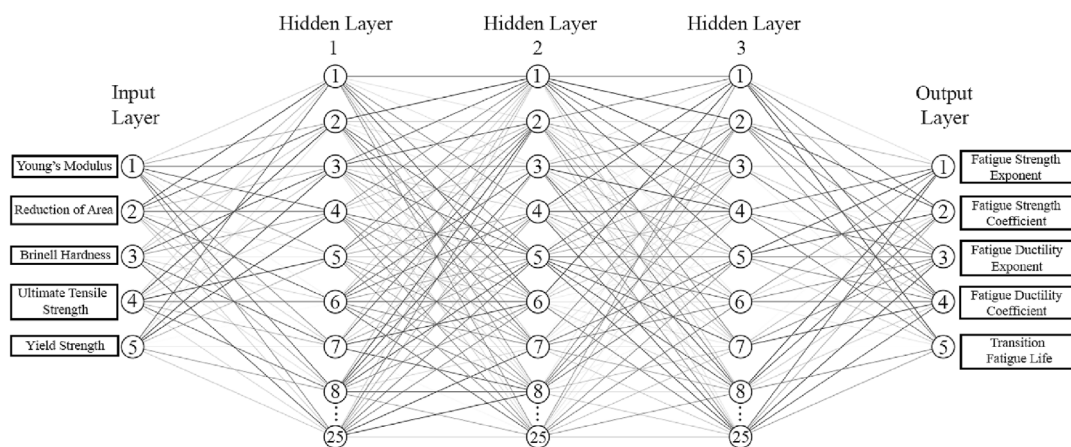


FIGURE 2 Structure of the ANN.

alongside various fatigue parameters. All the fatigue lives used in this study were calculated with Equation (1)⁴⁴:

$$(2N_t) = \left(\frac{\epsilon'fE}{\sigma'f} \right)^{\frac{1}{(b-c)}} \quad (1)$$

where b and c are the fatigue strength and ductility exponents, $\sigma'f$ and $\epsilon'f$ are the fatigue strength and ductility coefficients, E is Young's modulus, and N_t is the transition fatigue life. As seen in Figure 1, when the elastic strain amplitude is equal to the plastic strain

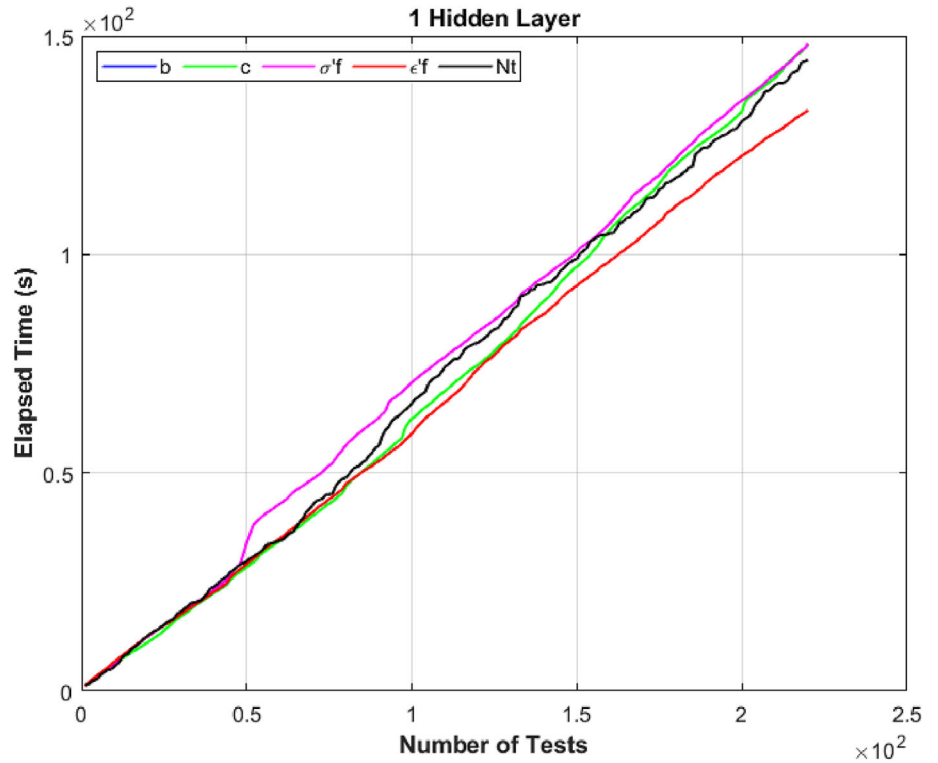


FIGURE 3 Comparison of the elapsed times of low-cycle fatigue parameters in one hidden layer structure. [Colour figure can be viewed at wileyonlinelibrary.com]

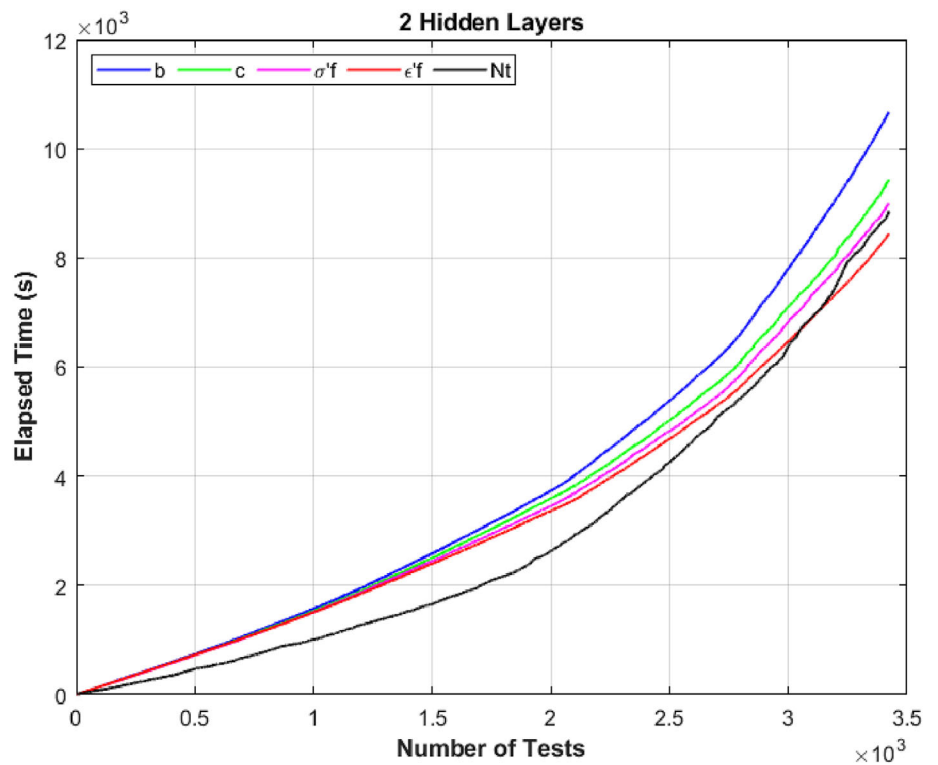


FIGURE 4 Comparison of the elapsed times of low-cycle fatigue parameters in two hidden layer structure. [Colour figure can be viewed at wileyonlinelibrary.com]

amplitude, transition fatigue life occurs at the intersection of the elastic and plastic strain lines.

Elastic strain is more prevalent on the left side of the transition fatigue life point and plastic strain is more prevalent on the right side of the transition fatigue life

point, which correspond to LCF and HCF regions respectively. Fatigue strength exponent and coefficient are determined via the elastic strain line and fatigue ductility exponent, and the coefficient is determined via the plastic strain line. Estimation of the fatigue transition point also

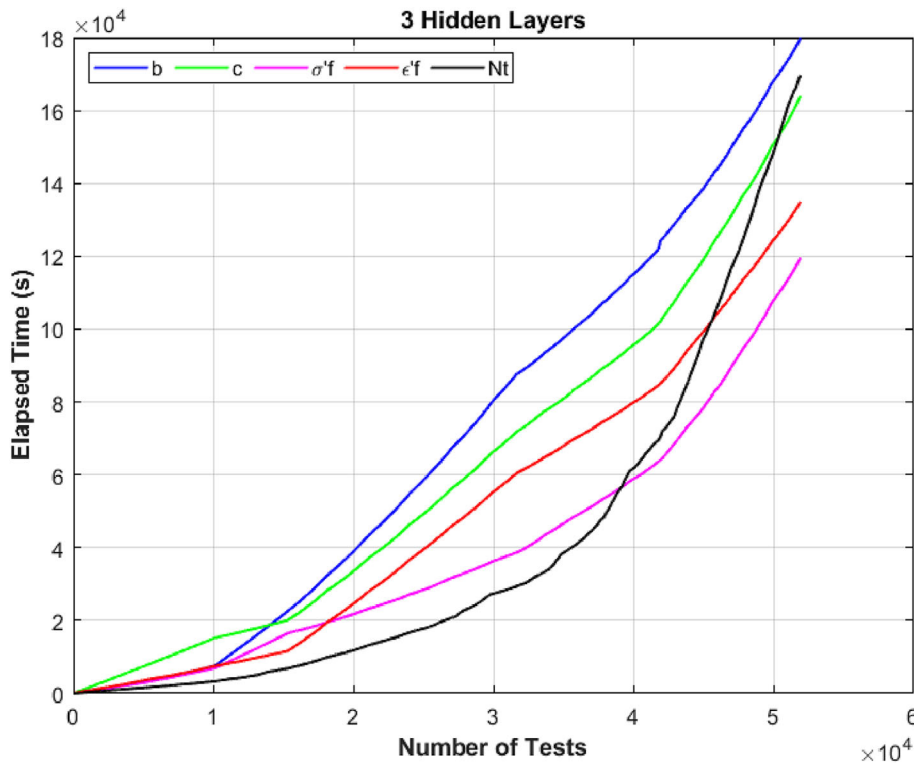


FIGURE 5 Comparison of the elapsed times of low-cycle fatigue parameters in three hidden layer structure. [Colour figure can be viewed at wileyonlinelibrary.com]

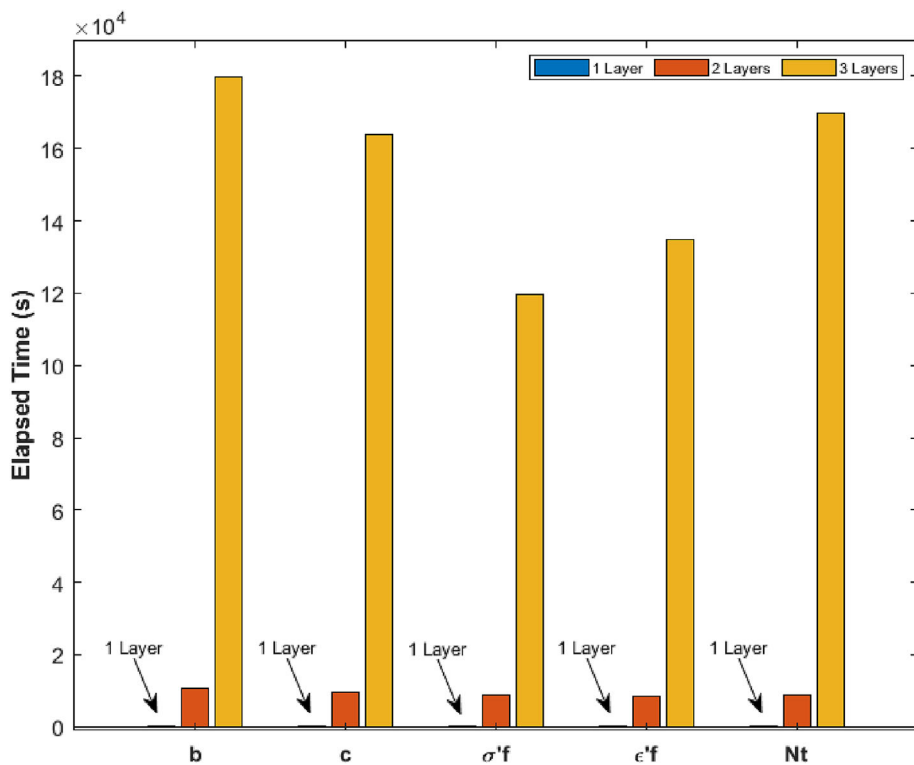


FIGURE 6 Comparison of the total elapsed times in one, two, and three hidden layer structures. [Colour figure can be viewed at wileyonlinelibrary.com]

TABLE 3 Best results belonging to the low-cycle fatigue parameters and transition fatigue life (b , c , $\sigma'f$, $\epsilon'f$, and N_t) with three hidden layers.

Parameter	Best range	Best MSE	Best regression	Average MSE	Average regression	HL1 neuron	HL1 neuron	HL2 neuron	HL2 neuron	HL3 neuron	HL3 activation function	HL2 activation function	HL1 activation function	HL3 activation function	Output activation function
b	10–15	1.8E – 05	0.971	3.1E – 05	0.954	15	15	10	10	15	Tansig	Purelin	Tansig	Tansig	Purelin
c	10–15	1.9E – 03	0.999	2.5E – 03	0.999	13	13	14	14	12	Logsig	Tansig	Logsig	Tansig	Tansig
$\sigma'f$	16–20	4.7E + 03	0.993	5.8E + 03	0.991	16	16	17	17	18	Purelin	Tansig	Purelin	Logsig	Purelin
$\epsilon'f$	10–15	7.0E – 03	0.968	1.1E – 02	0.951	15	15	12	12	11	Tansig	Purelin	Tansig	Tansig	Tansig
N_t	10–15	5.2E + 03	0.999	1.8E + 04	0.997	11	11	14	14	13	Purelin	Tansig	Purelin	Tansig	Tansig

TABLE 4 Best results belonging to the low-cycle fatigue parameters and transition fatigue life (b , c , $\sigma'f$, $\epsilon'f$, and N_t) with two hidden layers.

Parameter	Best range	Best MSE	Best regression	Average MSE	Average regression	HL1 neuron	HL1 neuron	HL2 neuron	HL2 neuron	HL3 neuron	HL3 activation function	HL2 activation function	HL1 activation function	HL3 activation function	Output activation function
b	10–15	4.0E – 05	0.934	5.4E – 05	0.92	10	10	14	14	14	Tansig	Logsig	Tansig	Logsig	Purelin
c	1–5	5.6E – 03	0.999	8.1E – 03	0.999	3	3	5	5	5	Logsig	Tansig	Logsig	Tansig	Purelin
$\sigma'f$	10–15	5.6E + 03	0.991	1.2E + 04	0.982	13	13	11	11	11	Tansig	Logsig	Tansig	Logsig	Purelin
$\epsilon'f$	16–20	1.7E – 02	0.935	2.3E – 02	0.908	20	20	19	19	19	Purelin	Logsig	Purelin	Logsig	Tansig
N_t	10–15	3.7E + 04	0.994	1.8E + 05	0.972	15	15	15	15	15	Purelin	Logsig	Purelin	Logsig	Tansig

allows accurate estimation of fatigue strength and fatigue ductility parameters.⁴⁶ Therefore, transition fatigue lives (N_t) are chosen for estimations.

In this study, changes in ANN parameters (hidden neuron numbers, HL numbers, and activation functions) and their effects on the LCF parameters of various steel alloys were investigated. In total, 73 steel alloys were used, and each of them used in this study was tested under fully reversed strains ($R = -1$). The tested strain amplitudes were ranging between 0.15% and 2%. The dataset was obtained from the literature^{44,47,48} and was previously published in Genel.³⁰ The modified dataset to include N_t is listed in Table A1. The estimated fatigue parameters are fatigue strength exponent (b), fatigue ductility exponent (c), fatigue strength coefficient ($\sigma'f$), fatigue ductility coefficient ($\epsilon'f$), and transition fatigue life (N_t). Five inputs were used: Young's modulus (E), reduction of area (RA%), Brinell hardness (BHN), yield strength (σ_y), and ultimate tensile strength (σ_u). The ANN approach was demonstrated to be an accurate and efficient method to estimate fatigue parameters in a previous study.⁶ The present paper serves as a continuation of the previous article and investigates the effect of increasing the HL numbers and activation functions on estimation accuracy on the LCF parameters. The main goal of this study is to recommend an optimal ANN structure without complexity by decreasing the hidden neuron and HL numbers, in addition to choosing the

most suitable activation functions in each layer for each estimation parameter. Thus, an ANN structure that is efficient in terms of both estimation time and accuracy can be used for selected LCF parameters.

2 | ANNs

ANNs can be used to solve complex problems with relative ease. The general ANN structure consists of three layers: input, hidden, and output. The ANN structure that has multiple HLs is called a DNN. Increasing the HL number deepens the network. The structure of the ANN used in this study is given in Figure 2. Used activation functions in this study are hyperbolic tangent sigmoid (tansig), logistic sigmoid (logsig), and linear (purelin) as they are commonly used in multilayer perceptron studies as previously mentioned. Levenberg–Marquardt (trainlm) is the most widely used training function and was selected as a backpropagation algorithm because it is relatively less memory-intensive in addition to reliable and rapid solutions relative to the other algorithms. Considering how much memory and training time are required as the HL number increases, the proper choice of training functions optimized for memory and time becomes essential. The maximum epoch number is set to 100; 75% of the data were used for training and 25% were used for testing. Normalization process made with MATLAB's

TABLE 5 Best results belonging to the low-cycle fatigue parameters and transition fatigue life (b , c , $\sigma'f$, $\epsilon'f$, and N_t) with one hidden layer.

Parameter	Best range	Best MSE	Best regression	Average MSE	Average regression	HL1 neuron	HL1 activation function	Output activation function
b	6–9	4.4E – 05	0.944	8.5E – 05	0.874	6	Logsig	Tansig
c	21–25	3.5E – 03	0.999	5.0E – 02	0.999	22	Purelin	Tansig
$\sigma'f$	6–9	6.8E + 03	0.989	3.4E + 04	0.944	6	Purelin	Tansig
$\epsilon'f$	10–15	1.6E – 02	0.929	3.7E – 02	0.857	10	Logsig	Tansig
N_t	16–20	1.7E + 04	0.972	3.3E + 04	0.921	19	Tansig	Tansig

Parameter	3 hidden layers	2 hidden layers	1 hidden layer
b	2.9	6.6	5.6
c	0.1	0.1	0.1
$\sigma'f$	0.7	0.9	1.1
$\epsilon'f$	3.2	6.5	7.1
N_t	0.1	0.6	2.8
Sum of elapsed times (s)	737	46,397	768,060
Sum of gaps (%)	7	14.7	16.7

TABLE 6 Differences between the sum of gaps and total elapsed times of low-cycle fatigue parameters and transition fatigue life in different hidden layers.

TABLE 7 The number of used activation functions for each parameter belonging to hidden layers and output layer.

3 hidden layers				2 hidden layers				1 hidden layer							
Parameter	Layer	Tansig	Logsig	Purelin	Parameter	Layer	Tansig	Logsig	Purelin	Parameter	Layer	Tansig	Logsig	Purelin	
<i>b</i>	HL1	204	160	136	<i>b</i>	HL1	202	175	123	<i>b</i>	HL1	26	24	0	
	HL2	193	195	112		HL2	209	243	48		Output	44	6	0	0
	HL3	167	267	66		Output	262	30	208		HL1	1	4	45	
<i>c</i>	Output	240	0	260	<i>c</i>	HL1	169	174	157	<i>c</i>	Output	25	21	4	4
	HL1	167	223	110		HL2	186	187	127		HL1	4	0	46	
	HL2	200	180	120		Output	142	142	216		Output	26	0	24	
$\sigma'f$	HL3	217	183	100	$\sigma'f$	HL1	181	161	158	$\sigma'f$	HL1	22	25	3	3
	Output	345	6	149		HL2	189	201	110		Output	41	3	6	6
	HL1	203	168	129		Output	197	0	303		HL1	21	17	12	
$\epsilon'f$	HL2	217	179	104	$\epsilon'f$	HL1	201	185	114	$\epsilon'f$	Output	29	0	21	21
	HL3	191	240	69		HL2	197	232	71		HL1	4	0	0	
	Output	169	0	331		Output	308	0	192		Output	21	17	12	
N_t	HL1	218	162	120	N_t	HL1	191	183	126	N_t	HL1	21	17	12	12
	HL2	202	197	101		HL2	197	226	77		Output	29	0	0	0
	HL3	204	228	68		Output	229	0	271		Output	29	0	0	0
N_t	Output	304	0	196	N_t	Output	229	0	271	N_t	Output	29	0	0	0
	HL1	183	197	120		HL1	191	183	126		Output	29	0	0	0
	HL2	188	180	132		HL2	197	226	77		Output	29	0	0	0
N_t	HL3	212	207	81	N_t	Output	229	0	271	N_t	Output	29	0	0	0
	Output	304	0	196		Output	229	0	271		Output	29	0	0	0

“mapminmax” function ranges between $[-1,1]$. Mean squared error (MSE) is selected as the error function. The following basic material properties are selected as inputs: Young's modulus (E), reduction of area (RA%), Brinell hardness (BHN), yield strength (σ_y), and ultimate tensile strength (σ_u). The following LCF parameters are selected as outputs: fatigue strength exponent (b), fatigue strength coefficient (σ'_f), fatigue ductility exponent (c), fatigue ductility coefficient (ϵ'_f), and transition fatigue life (N_t).

All the tests were performed on the MATLAB R2022a software with an i3-1115G4 3.00 GHz processor, 8 GB RAM, 3500–2500 MB/s read/write NVMe M.2 SSD, and Windows 10 operating system. A summary of the ANN structure parameters is given in Table 2.

3 | RESULTS AND DISCUSSION

3.1 | Comparison of the elapsed times in different HL numbers

Elapsed time represents how long the algorithm ran from beginning to end. Elapsed time is a highly important parameter and can be correlated to performance. Generally, the main goal is to increase the estimation accuracy while lowering estimation time. Comparisons of the elapsed times of LCF parameters in one, two, and three HL structures are given in Figures 3–5, respectively.

Changes in the ANN structure are considered the main reason for the increase in the elapsed time. Parameters affecting the elapsed time are hidden neuron

number, number of HLs, and activation functions in the HL and output layer. One HL structure consists of one hidden neuron (HL1) and two activation function (HL1 and output layer) combinations. For two HL structure, there are two hidden neurons (HL1 and HL2) and three activation function (HL1, HL2, and output layer) combinations. For three HL structure, there are three hidden neurons (HL1, HL2, and HL3) and four activation function (HL1, HL2, HL3, and output layer) combinations. With the increase of the hidden neuron numbers and HLs, the elapsed time increases since each layer of the network computes all the weights and biases by activation functions. Also, increased neuron numbers of the more complex network structures were significantly affecting the computing time. As expected, with the more structural complexity, the elapsed time has drastically increased. Comparisons of total elapsed times considering Figures 3–5 (including all LCF parameters and transition fatigue life) for one, two, and three HL structures were presented in Figure 6.

There is a huge difference in the elapsed times between the HL changes. The three HL structure requires more time and higher amounts of computing power. However, the one HL structure takes less time and computing power. There are significant elapsed time differences between the output parameters. The highest to lowest elapsed times of the output parameters were fatigue strength exponent, transition fatigue life, fatigue ductility exponent, fatigue ductility coefficient, and fatigue strength coefficient, respectively. Normally, it does not take this much time to estimate the parameters,

TABLE 8 The total number of used activation functions in the hidden layers and the output layer for each parameter.

b	Tansig	Logsig	Purelin	c	Tansig	Logsig	Purelin
HL1	432	359	259	HL1	337	401	312
HL2	446	444	160	HL2	411	388	251
HL3	429	297	274	HL3	359	325	316
Output	240	0	260	Output	345	6	149
σ'_f	Tansig	Logsig	Purelin	ϵ'_f	Tansig	Logsig	Purelin
HL1	388	329	333	HL1	441	372	237
HL2	432	380	238	HL2	440	432	178
HL3	388	240	372	HL3	512	228	260
Output	169	0	331	Output	304	0	196
N_t	Tansig	Logsig	Purelin	General	Tansig	Logsig	Purelin
HL1	395	397	258	HL1	1598	1461	1141
HL2	414	406	230	HL2	1729	1644	827
HL3	441	207	352	HL3	1688	1090	1222
Output	304	0	196	Output	1058	6	936

but experimental studies must be made for increasing the prediction accuracy and seeing the neural network structure hyperparameter effects on the estimated parameters. Each network structure component, such as function, layer, and neurons, affects the results directly. This “trial-and-error” approach is required to determine the best and most robust network structure. The present study assists in understanding the ANN structure parameters and serves as a guide for researchers who want to estimate the LCF parameters using neural networks.

3.2 | LCF parameter estimation results and comparison of the activation functions in different HL numbers

MATLAB toolbox has several activation functions such as hyperbolic tangent sigmoid (tansig), logistic sigmoid (logsig), linear (purelin), positive linear (poslin), positive hard limit (hardlim), triangular basis (tanbas), and so forth. Aside from these functions, there are several activation functions that are not part of the MATLAB toolbox library like rectified linear unit (ReLU), leaky ReLU (Leaky ReLU), parametric ReLU (PReLU), randomized leaky ReLU (RRReLU), and exponential linear unit (ELU). In order to ensure ease of use and accessibility for the network structure, only the most used activation functions (tansig, logsig, and purelin) of the MATLAB toolbox library were tested. This choice of activation functions also aligns with the goal of simplifying ANN structure and eliminating complexity. The hidden neuron numbers were selected within the range of 1–25 hidden neurons. In order to find the best suitable hidden neuron number range for the specified HL numbers, the hidden neuron range was divided into five parts: 1–5, 6–9, 10–15, 16–20, and 21–25. Additionally, CPU power, RAM usage, and time considerably rose with the increasing number of HLs and hidden neuron numbers, as anticipated. Average MSE and regression values of the current HL number and hidden neuron range are called average MSE and average regression, respectively. Average MSE and regression values were calculated with the average of the best 10 values belonging to the hidden neuron range. The best range was determined with the hidden neuron range that has the lowest average MSE and the highest regression value. The hidden neuron is unavailable in the input and output layers, and the activation function is also unavailable in the input layer. Three different layers, activation functions, and 25 different hidden neurons were tested in the present study. The best combinations belonging to the LCF parameters and transition fatigue life with three HLs, two HLs, and one HL were presented in Tables 3–5, respectively.

As mentioned before, increasing the HL number increases the estimation accuracy. The lowest MSE and the highest regression values were obtained in the three HLs. When the regression value is reached “1,” then the maximum estimation accuracy is obtained. The percentage difference between the best regression values of the estimated parameters and the maximum regression value is named the “gap.” The gap values and total elapsed times (sum of the elapsed times of b , c , $\sigma'f$, $\epsilon'f$, and N_t) are given in Table 6. Regression values of the LCF parameters and transition fatigue life show no significant difference with the increase in the HL number. Therefore, the higher number of HLs cannot be justified with small differences in regression since the elapsed time difference was overwhelmingly huge.

It should be noted that individual best results are not a good enough indication for determining the best hidden neuron range and activation functions because even if nothing changes, the ANN results differ on each run. Therefore, the best average results must be considered. Replication can be performed to prevent the difference; however, replication was not performed in the present study due to time limitations. The full factorial experiment of three HLs took 598,380 s (~7 days), and this value is multiplied by the number of replications. For 100 replications, three HLs with three different activation functions and five different hidden neuron parts ranging from 1 to 25 hidden neurons would take about 70 days, two HLs 43 days, and one layer less than 1 day. For this reason, one HL is deemed sufficient for the estimation problems. Changing the ANN parameters and specializing the network for the estimation problem with one HL are more reasonable in terms of time, complexity, and knowledge. Our previous work⁶ is supporting these inferences.

Each HL and output layer includes three activation functions, and each HL consists of 25 hidden neurons. For each parameter, if the hidden neuron range was not divided into five parts, $25 \times 25 \times 25 \times 3 \times 3 \times 3 \times 3 = 1,265,625$ results would have been obtained for three HLs and 16,875 for two HLs. By dividing the hidden neuron range, the resulting number was reduced to 53,055 for three and 3429 for two HLs, respectively. One HL result numbers did not change because of consisting only one HL. The best hundred values that have the highest regression and the lowest MSE in three and two HLs were separated. Then the number of activation functions and hidden neurons was counted via Excel. For one HL, the best 10 values were considered because the total number of the results belonging to each parameter was below a hundred. The number of used activation functions for each parameter belonging to HLs and output layer is provided in Table 7.

The total number of used activation functions in the HLs and the output layer for each parameter is given in Table 8. The “General” in this context represents the total of all estimation parameters (b , c , $\sigma'f$, $\epsilon'f$, and N_t).

3.2.1 | Output layer

For one HL, fatigue strength exponent (b) was highly dependent on tansig, fatigue ductility exponent (c) was dependent on tansig and logsig, fatigue strength coefficient ($\sigma'f$) was dependent on tansig and purelin, fatigue ductility coefficient ($\epsilon'f$) was highly dependent on tansig, and transition fatigue life (N_t) was dependent on tansig and purelin. For two HLs, b was dependent on tansig and purelin, c was dependent on purelin, $\sigma'f$ was highly dependent on purelin, $\epsilon'f$ was highly dependent on tansig, and N_t was dependent on tansig and purelin. For three HLs, b was dependent on tansig and purelin, c was highly dependent on tansig, $\sigma'f$ was highly dependent on purelin, $\epsilon'f$ was highly dependent on tansig, and N_t was highly dependent on tansig. The logistic sigmoid activation function (logsig) rarely performed well in the output layers, and the results

have shown that logsig is not suitable in the output layer for all estimation parameters. Logsig only performed well in the one and two HL configurations for fatigue ductility exponent (c).

3.2.2 | HLs

In HLs, b , c , $\sigma'f$, $\epsilon'f$, and N_t showed good agreement with tansig and logsig, and tansig performed a little better than the logsig. As seen in Table 1, for many authors, purelin was chosen only in the output layer. The total percentage values of the used activation functions of estimated parameters and general with the HLs and the output layer are given in Figure 7.

3.3 | Determining the best hidden neuron number range

The hidden neuron number is a highly important hyperparameter, and it is difficult to determine the best range. Unsurprisingly, an increase in the hidden neuron increases the complexity and elapsed time. It is also worth

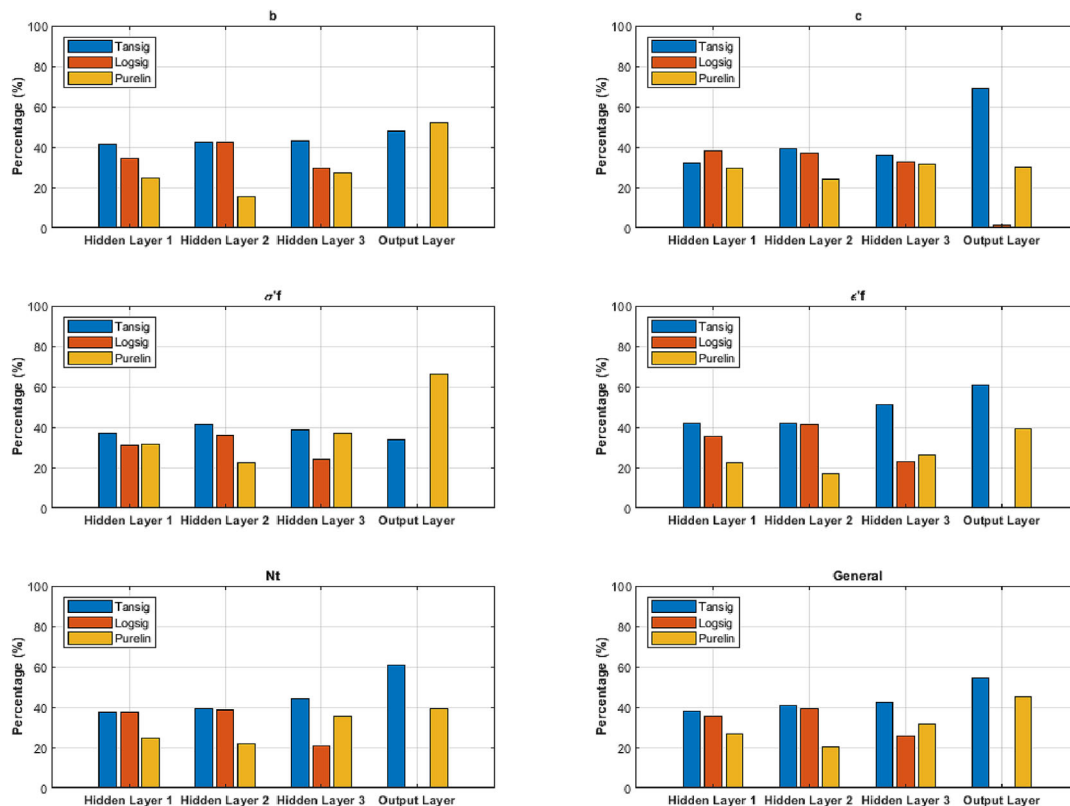


FIGURE 7 The total percentage values of the used activation functions of estimated parameters and general. [Colour figure can be viewed at [wileyonlinelibrary.com](https://onlinelibrary.wiley.com/doi/10.1111/ffe.14054)]

mentioning that there is no upper or lower limit to the hidden neuron number. As stated before, recommendations for the HL are the same for the hidden neuron number as well; it should not be increased unnecessarily. Also, there is no theoretical basis between the hidden neuron number and the estimation accuracy. Each input parameter, output parameter, data size, activation function, and training function behave differently according to the increase/decrease of the hidden neuron number, so estimation problems and their parameters must be specialized according to the network. There is no exactly a “true” hidden neuron value or HL value for all types of problems, but there are some tips and suggestions about which is worse or better in certain conditions for ANN investigations. The best 100 results for each hidden neuron range (1–5, 6–9, 10–15, 16–20, and 21–25) belonging to each parameter were selected and counted the number of the best performed hidden neurons in HLs. Figure 8 shows the number of used hidden neurons for estimation parameters in all HLs.

The best range has been found to be within “4–9” and the second-best range within “22–25” for all estimation parameters and HLs, but the best average results have been obtained within “10–15” hidden neurons. “4–9” and “22–25” were the most used ranges for the best hundred results, but the best 10 results were obtained in the “10–15” hidden neuron range.

Selecting the right parameters for the network is the most important factor in obtaining highly accurate results in a reasonable estimation time. At first, estimation accuracy can seem to be directly proportional to the HL and hidden neuron number. However, unnecessarily increasing the hidden neuron and HL causes structural complexity and a high amount of estimation time without a significant increase in the estimation accuracy. For

evaluations of inherently complex LCF parameters, which already require time-intensive testing processes, using an equally time-consuming ANN structure mostly defeats the purpose without adequate results. Therefore, it is imperative to choose the optimal HL, hidden neuron numbers, and activation function combinations to ensure rapid and accurate estimations.

3.4 | Comparison of the estimated and experimental parameter values

ANN structure and its results give highly important information about how good the estimation results are with the MSE and regression values. To further demonstrate the estimation quality, comparisons of estimated data of one, two, and three HLs were provided along with experimental values in the form of graphs. Comparisons of estimated and experimental parameters values (b , c , $\sigma'f$, $\epsilon'f$, and N_t) are given in Figures 9–13, respectively. Estimated parameter values are obtained from the ANN structure with the best results. Percentage errors are calculated with mean absolute percentage error (MAPE), which is given in Equation (2):

$$MAPE = \frac{100}{N} \sum_1^N \frac{|V_{\text{true}} - V_{\text{estimated}}|}{V_{\text{true}}} \quad (2)$$

where V_{true} is the true value of the parameter, $V_{\text{estimated}}$ is the estimated value of the parameter, N is the number of observations, and “100” is to convert results to percentages. MAPE results of three, two, and one HL structures belonging to the estimated parameters are given in Table 9.

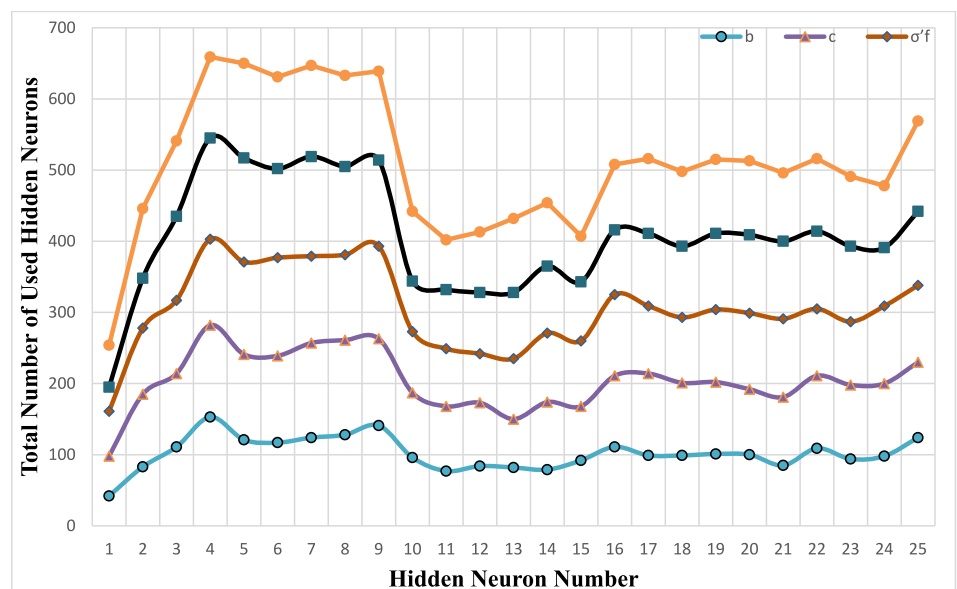


FIGURE 8 The number of used hidden neurons for estimation parameters in all hidden layers. [Colour figure can be viewed at wileyonlinelibrary.com]

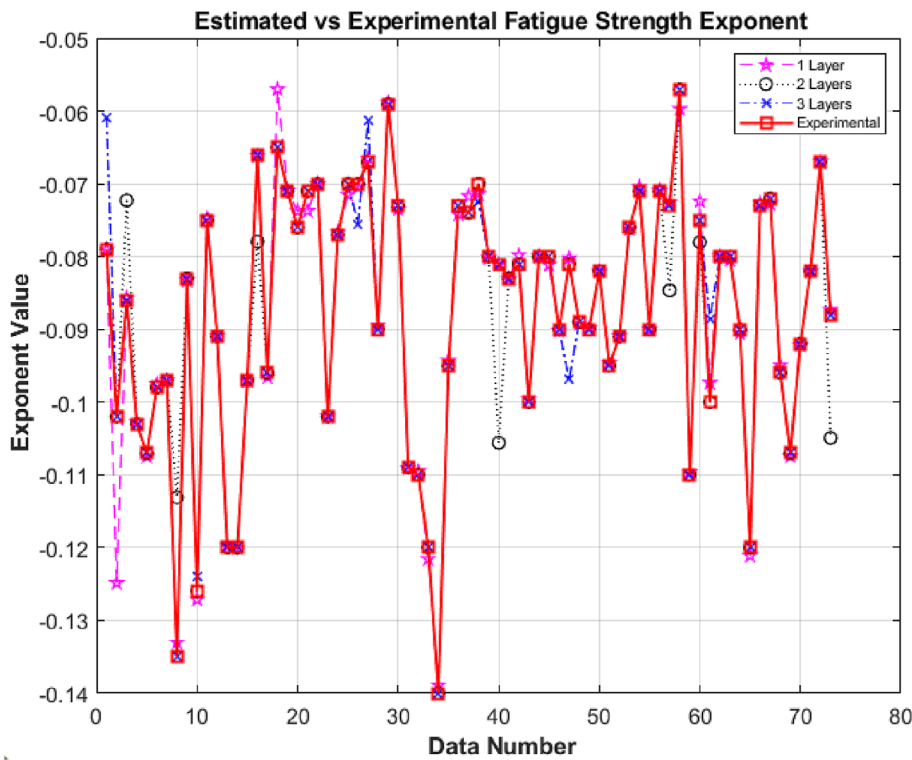


FIGURE 9 Comparison of estimated and experimental values of fatigue strength exponent (b). [Colour figure can be viewed at wileyonlinelibrary.com]

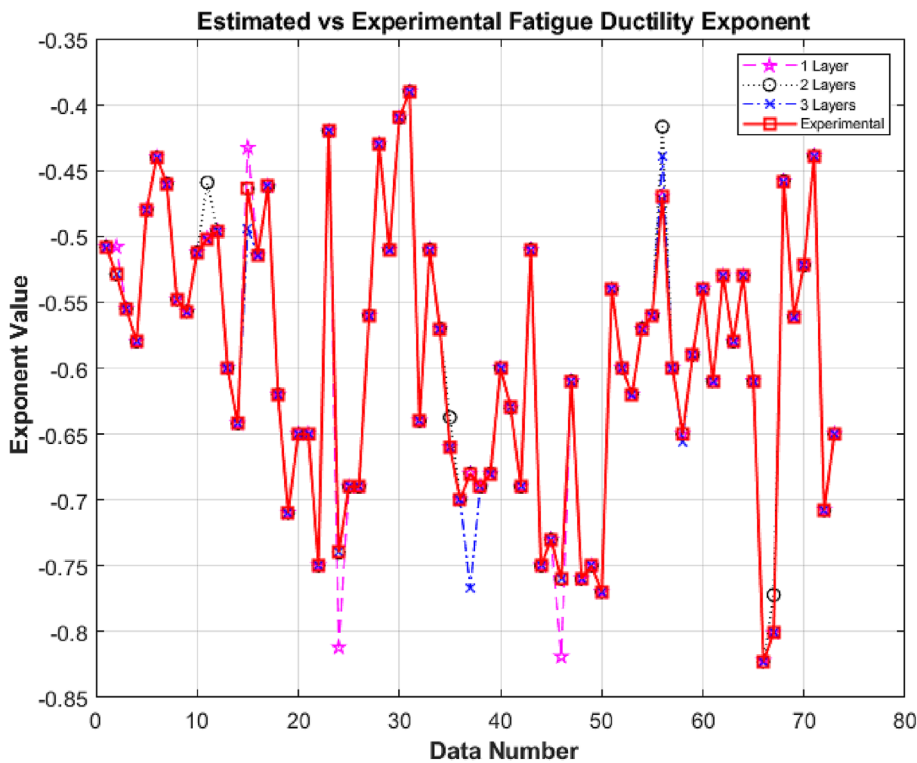


FIGURE 10 Comparison of estimated and experimental values of fatigue ductility exponent (c). [Colour figure can be viewed at wileyonlinelibrary.com]

In addition to considering Figure 9, three HL structure gave the best MAPE result. However, there was no considerable difference between the three HL and one HL structures. Additionally, three HL structure requires a lot of time, computational power, and structural

complexity. For these reasons, selecting the one HL structure is considered a better choice.

Fatigue ductility exponent resulted in the lowest MAPE values compared to all estimation parameters, and one HL structure performed the best. Figure 10 shows

FIGURE 11 Comparison of estimated and experimental values of fatigue strength coefficient (σ'_f). [Colour figure can be viewed at wileyonlinelibrary.com]

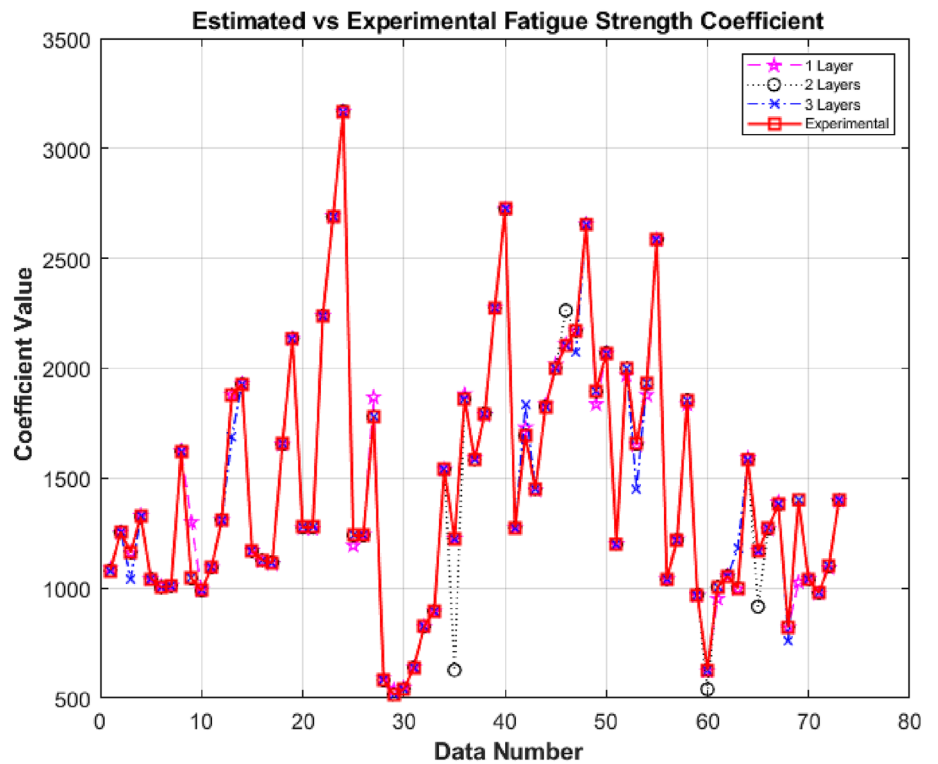
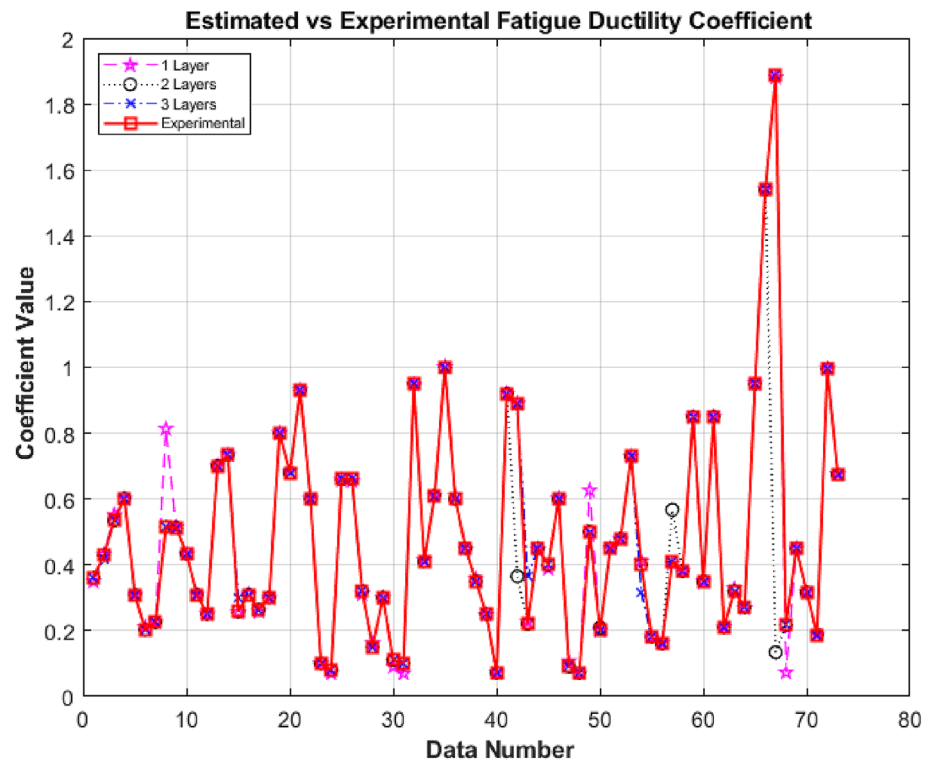


FIGURE 12 Comparison of estimated and experimental values of fatigue ductility coefficient (ϵ'_f). [Colour figure can be viewed at wileyonlinelibrary.com]



that the estimated fatigue ductility exponent mostly coincides with the experimental values, confirming the low MAPE value.

MAPE value of three HL structure was the lowest for fatigue strength coefficient. However, the difference between MAPE values between one, two, and three

HL structures was not high enough to warrant increased estimation time. Figure 11 similarly shows the estimation quality of the structures. Several differences can be seen between estimated and experimental values. However, they mostly coincide or remain within an acceptable margin of the experimental values.

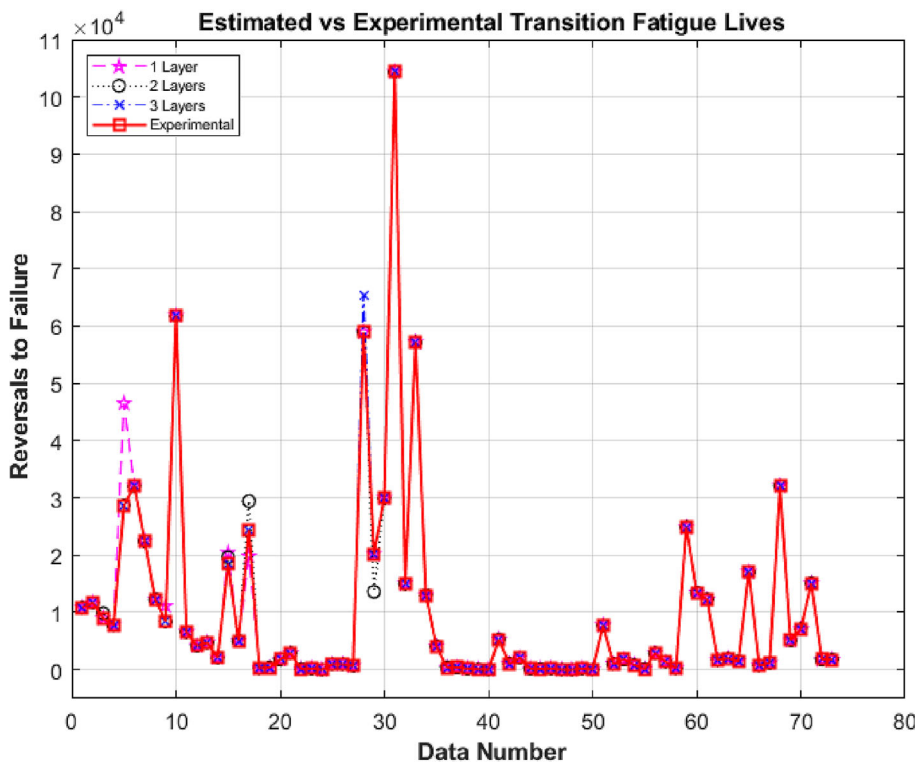


FIGURE 13 Comparison of estimated and experimental values of transition fatigue life (N_t). [Colour figure can be viewed at [wileyonlinelibrary.com](https://onlinelibrary.wiley.com)]

Parameter	3 hidden layers	2 hidden layers	1 hidden layer
b	1.035	1.641	1.206
c	0.326	0.411	0.285
σ_f	0.969	1.261	1.334
ϵ'_f	1.461	2.686	3.904
N_t	0.573	0.944	1.695

TABLE 9 MAPE results of the estimated parameters (b , c , σ'_f , ϵ'_f , and N_t).

Compared to other estimation parameters, the MAPE results of the fatigue ductility coefficient are relatively high. Three HL structure provided the best result, while one HL structure performed relatively poorly. Despite its disadvantages, three HL structure should be preferred for the fatigue ductility coefficient to ensure estimation accuracy. Figure 12 shows the difference between estimated and experimental data with three HL data points coinciding with experimental ones.

Once again, three HL structure performed the best for fatigue life as well in terms of MAPE values. There were relatively high differences between the layers. One HL performed the worst result when MAPE values were compared. However, as seen in Figure 13, only one clearly visible point seems to be responsible for the high MAPE value. For this reason, choosing the best HL combination might be difficult. MSE, regression, time, complexity, computational power, and MAPE difference between the experimental and estimated values must be

considered together while selecting the best structure for estimation parameters.

4 | CONCLUSIONS

In this work, LCF parameters and transition fatigue life have been estimated by the ANN approach. Also, different HLs (one, two, and three), activation functions (tansig, logsig, and purelin), and hidden neurons (1–25) and their effects on the estimation accuracy, MSE, and elapsed time have been investigated. Increasing the HL increased the estimation accuracy at the cost of drastically increasing elapsed time. There was no direct consistent correlation between the hidden neuron increase and estimation accuracy. Three activation functions were tested in different HLs with different hidden neurons. The results have shown that the most suitable activation functions for the output layer were firstly the hyperbolic

tangent sigmoid (tansig) and secondly the linear (purelin) activation functions in one, two, and three HL structures. On the other hand, the logistic sigmoid activation function never performed well in the output layer. For the HLs, tansig resulted in the best solutions in comparison to the results of logsig and purelin. Purelin can be used in the HLs, but it is not preferred as linearity is mostly needed in the output layer. The best structure for the three hidden layered was tansig–tansig–tansig/purelin and 10–15 hidden neurons in each HL, for two hidden layered was tansig–logsig–purelin/tansig and 10–15 hidden neurons, and for one hidden layered was purelin–tansig and 1–5 hidden neurons. Although the three HLs resulted in better regression and lower MSE values, there is no significant difference between the one HL structure. The disadvantages of the three HLs are significant differences in the elapsed time and more structural complexity. As a result, one HL structure provides less structural complexity, knowledge, computation time, and power. Also, estimated and experimental parameter values showed good agreement in terms of small mean absolute percentage errors.

In the future, the authors intend to expand the use of the optimized ANN structures in the evaluation of fatigue parameters by performing estimations for different materials and structures. Additionally, optimization of ANN structure for other energy parameters should be considered as future research.

NOMENCLATURE

ANN	artificial neural network
b	fatigue strength exponent
BHN	Brinell hardness
c	fatigue ductility exponent
DNN	deep neural network
E	Young's modulus
elliotsig	Elliot symmetric sigmoid activation function
ELU	exponential linear unit
hardlim	hard limit activation function
HCF	high-cycle fatigue
HL	hidden layer
logsig	logistic sigmoid activation function
MLP	multilayer perceptron
MSE	mean squared error
N_t	transition fatigue life
poslin	positive linear activation function
PReLU	parametric rectified linear unit
purelin	linear activation function
RA%	reduction of area
ReLU	rectified linear unit
RReLU	randomized leaky rectified linear unit
tanbas	triangular basis activation function
tansig	hyperbolic tangent sigmoid activation function
trainlm	Levenberg–Marquardt training function

$V_{\text{estimated}}$	estimated value of the parameter
V_{true}	true value of the parameter
$\epsilon'f$	fatigue ductility coefficient
$\sigma'f$	fatigue strength coefficient
σ_u	ultimate tensile strength
σ_y	yield strength

DATA AVAILABILITY STATEMENT

Research data are not shared.

ORCID

Filippo Berto  <https://orcid.org/0000-0001-9676-9970>

REFERENCES

- Pareek VK, Brungs MP, Adesina AA, Sharma R. Artificial neural network modeling of a multiphase photodegradation system. *J Photochem Photobiol A Chem.* 2002;149(1–3):139–146.
- Collins W, Tissot P. An artificial neural network model to predict thunderstorms within 400 km² South Texas domains. *Meteorol Appl.* 2015;22(3):650–665.
- Al-kaf HAG, Chia KS, Alduais NAM. A comparison between single layer and multilayer artificial neural networks in predicting diesel fuel properties using near infrared spectrum. *Pet Sci Technol.* 2018;36(6):411–418.
- Uzair M, Jamil N. Effects of hidden layers on the efficiency of neural networks. In: *2020 IEEE 23rd International Multitopic Conference (INMIC).* IEEE; 2020:1–6.
- Tran TTK, Lee T, Kim JS. Increasing neurons or deepening layers in forecasting maximum temperature time series? *Atmos.* 2020;11(10):1072.
- Soyer MA, Kalaycı CB, Karakaş Ö. Low-cycle fatigue parameters and fatigue life estimation of high-strength steels with artificial neural networks. *Fatigue Fract Eng Mater Struct.* 2022; 45(12):3764–3785.
- Hojjat M. Modeling heat transfer of non-Newtonian nanofluids using hybrid ANN-metaheuristic optimization algorithm. *J Particle Sci Technol.* 2017;3(4):233–241.
- Raghu S, Sriraam N. Optimal configuration of multilayer perceptron neural network classifier for recognition of intracranial epileptic seizures. *Expert Syst Appl.* 2017;89:205–221.
- Rezaeian Zadeh M, Amin S, Khalili D, Singh VP. Daily outflow prediction by multi layer perceptron with logistic sigmoid and tangent sigmoid activation functions. *Water Res Manag.* 2010; 24(11):2673–2688.
- Altikat S. Prediction of CO₂ emission from greenhouse to atmosphere with artificial neural networks and deep learning neural networks. *Int J Environ Sci Technol.* 2021;18(10):3169–3178.
- Karsoliya S. Approximating number of hidden layer neurons in multiple hidden layer BPNN architecture. *Int J Eng Trends Technol.* 2012;3(6):714–717.
- Shen Z, Yang H, Zhang S. Neural network approximation: three hidden layers are enough. *Neural Netw.* 2021;141:160–173.
- Kalaycı CB, Karagöz S, Karakaş Ö. Bee colony intelligence in fatigue life estimation of simulated magnesium alloy welds. *Int J Fatigue.* 2019;127:36–44.
- Karakaş Ö, Canyurt OE, Gulsoz A. Fatigue strength estimation of butt welded joints in magnesium AZ31 alloy using the genetic algorithm. *Materialwiss Werkstofftech.* 2008;39(3):234–240.

15. Zhou N, Zhang J, Ju F, Liu S. Genetic algorithm coupled with the neural network for fatigue properties of welding joints predicting. *J Comput.* 2012;7(8):1887-1894.
16. Zeng F, Yang Y, Qian G. Fatigue properties and SN curve estimating of 316L stainless steel prepared by SLM. *Int J Fatigue.* 2022;162:106946.
17. Moghaddam TB, Soltani M, Shahraki HS, Shamshirband S, Noor NBM, Karim MR. The use of SVM-FFA in estimating fatigue life of polyethylene terephthalate modified asphalt mixtures. *Measurement.* 2016;90:526-533.
18. Karakaş Ö, Berto F, Hong Y. Fatigue & Fracture of Engineering Materials & Structures Virtual Special Issue: data science and machine learning for fatigue and fracture assessment. *Fatigue Fract Eng Mater Struct.*
19. Feng J, Lu S. Performance analysis of various activation functions in artificial neural networks. In: *Journal of Physics: Conference Series* (Vol. 1237, No. 2, p. 022030). IOP Publishing; 2019.
20. Maleki E, Unal O, Seyedi Sahebari SM, Reza Kashyzadeh K, Danilov I. Application of deep neural network to predict the high-cycle fatigue life of AISI 1045 steel coated by industrial coatings. *J Mar Sci Eng.* 2022;10(2):128.
21. Burghardt R, Wächter M, Masendorf L, Esderts A. Estimation of elastic-plastic notch strains and stresses using artificial neural networks. *Fatigue Fract Eng Mater Struct.* 2021;44(10):2718-2735.
22. Muñoz-Abella B, Rubio L, Rubio P. Stress intensity factor estimation for unbalanced rotating cracked shafts by artificial neural networks. *Fatigue Fract Eng Mater Struct.* 2015;38(3):352-367.
23. Xu T, Ding S, Zhou H, Li G. Machine learning-based efficient stress intensity factor calculation for aeroengine disk probabilistic risk assessment under polynomial stress fields. *Fatigue Fract Eng Mater Struct.* 2022;45(2):451-465.
24. Zhou K, Sun X, Shi S, Song K, Chen X. Machine learning-based genetic feature identification and fatigue life prediction. *Fatigue Fract Eng Mater Struct.* 2021;44(9):2524-2537.
25. Rubio P, Muñoz-Abella B, Rubio L. Neural approach to estimate the stress intensity factor of semi-elliptical cracks in rotating cracked shafts in bending. *Fatigue Fract Eng Mater Struct.* 2018;41(3):539-550.
26. Yetilmezsoy K, Demirel S. Artificial neural network (ANN) approach for modeling of Pb(II) adsorption from aqueous solution by Antep pistachio (*Pistacia Vera* L.) shells. *J Hazard Mater.* 2008;153(3):1288-1300.
27. Turp SM, Eren B, Ates A. Prediction of adsorption efficiency for the removal of nickel(II) ions by zeolite using artificial neural network (ANN) approach. *Fresen Environ Bull.* 2011;20(12):3158-3165.
28. Nejad RM, Sina N, Ma W, Liu Z, Berto F, Gholami A. Optimization of fatigue life of pearlitic Grade 900A steel based on the combination of genetic algorithm and artificial neural network. *Int J Fatigue.* 2022;162:106975.
29. Zhang J, Zhu J, Guo W, Guo W. A machine learning-based approach to predict the fatigue life of three-dimensional cracked specimens. *Int J Fatigue.* 2022;159:106808.
30. Genel K. Application of artificial neural network for predicting strain-life fatigue properties of steels on the basis of tensile tests. *Int J Fatigue.* 2004;26(10):1027-1035.
31. Pujol JCF, Pinto JMA. A neural network approach to fatigue life prediction. *Int J Fatigue.* 2011;33(3):313-322.
32. Maleki E, Unal O, Kashyzadeh KR. Fatigue behavior prediction and analysis of shot peened mild carbon steels. *Int J Fatigue.* 2018;116:48-67.
33. Sulaiman SI, Rahman TA, Musirin I, Shaari S. Performance analysis of evolutionary ANN for output prediction of a grid-connected photovoltaic system. *Int J Electr Comput Eng.* 2009; 3(5):1196-1202.
34. Kalayci CB, Karagoz S, Karakas Ö. Soft computing methods for fatigue life estimation: a review of the current state and future trends. *Fatigue Fract Eng Mater Struct.* 2020;43(12):2763-2785.
35. Boob G, Deoghare AB. Estimation of strain controlled fatigue properties of steels using tensile test data. In: *International and 16th National Conference on Machines and Mechanisms (INaCoMM2013)*. IIT Roorkee; 2013.
36. Suvvari N, Srinadh KS. Artificial neural network technique as a method to evaluate the strain-life fatigue properties of steel weldments on the basis of tensile tests. ICARMMIEM-2014. 2014.
37. Karakas Ö. Estimation of fatigue life for aluminium welded joints with the application of artificial neural networks. *Materiawiss Werkstofftech.* 2011;42(10):888-893.
38. Karakas Ö, Tomasella A. Fatigue life estimation of non-penetrated butt weldments in light metals by artificial neural network approach. *Materiawiss Werkstofftech.* 2013;44(10):847-855.
39. Barbosa JF, Correia JA, Júnior RF, De Jesus AM. Fatigue life prediction of metallic materials considering mean stress effects by means of an artificial neural network. *Int J Fatigue.* 2020;135:105527.
40. Ghajar R, Alizadeh KJ, Naserifar N. Estimation of cyclic strain hardening exponent and cyclic strength coefficient of steels by artificial neural networks. In: *ASME International Mechanical Engineering Congress and Exposition*, Vol. 48739; 2008:639-648.
41. Ghajar R, Naserifar N, Sadati H, Alizadeh KJ. A neural network approach for predicting steel properties characterizing cyclic Ramberg-Osgood equation. *Fatigue Fract Eng Mater Struct.* 2011;34(7):534-544.
42. Janežič M, Klemenc J, Fajdiga M. A neural-network approach to describe the scatter of cyclic stress-strain curves. *Mater Des.* 2010;31(1):438-448.
43. Tomasella A, El Dsoki C, Hanselka H, Kaufmann H. A computational estimation of cyclic material properties using artificial neural networks. *Procedia Eng.* 2011;10:439-445.
44. Roessle ML, Fatemi A. Strain-controlled fatigue properties of steels and some simple approximations. *Int J Fatigue.* 2000; 22(6):495-511.
45. McKeen LW. Introduction to fatigue and tribology of plastics and elastomers. *Fatigue Tribol Prop Plastics Elastom.* 2010;1:1-23.
46. Williams CR, Lee YL, Rilly JT. A practical method for statistical analysis of strain-life fatigue data. *Int J Fatigue.* 2003;25(5):427-436.
47. SAE J1099 Committee. Technical report on fatigue properties. SAE J1099, Society of Automotive Engineers, Warrendale, PA; 1975.
48. Kim KS, Chen X, Han C, Lee HW. Estimation methods for fatigue properties of steels under axial and torsional loading. *Int J Fatigue.* 2002;24(7):783-793.

How to cite this article: Soyer MA, Tüzün N, Karakaş Ö, Berto F. An investigation of artificial neural network structure and its effects on the estimation of the low-cycle fatigue parameters of various steels. *Fatigue Fract Eng Mater Struct.* 2023; 46(8):2929-2948. doi:10.1111/ffe.14054

APPENDIX A

TABLE A1 Monotonic, low-cycle fatigue, and transition fatigue properties of various steel alloys used in this study.

Steel type	E (GPa)	RA (%)	σ_u (MPa)	BHN (kgf/mm ²)	σ_y (MPa)	b	c	σ'_f (MPa)	ϵ'_f	N_t (cycles)	Ref.
1141	217	54	802	241	602	-0.079	-0.508	1080	0.361	10,862	44
1141	214	49	725	217	450	-0.102	-0.529	1255	0.43	11,674	44
1141	215	58	797	252	610	-0.086	-0.555	1162	0.534	8958	44
1141	220	47	789	229	493	-0.103	-0.58	1326	0.602	7776	44
1038	201	54	582	163	331	-0.107	-0.48	1043	0.309	28,664	44
1038	219	53	652	185	359	-0.098	-0.44	1004	0.202	32,075	44
1038	219	67	649	195	410	-0.097	-0.46	1009	0.225	22,446	44
1541	205	55	783	180	475	-0.135	-0.548	1622	0.515	12,304	44
1541	205	42	906	195	475	-0.083	-0.557	1044	0.513	8415	44
1050	211	50	821	205	465	-0.126	-0.512	989	0.433	61,820	44
1050	203	34	829	220	460	-0.075	-0.502	1094	0.309	6563	44
1090	203	14	1090	259	735	-0.091	-0.496	1310	0.25	4172	44
1090	217	22	1147	309	650	-0.12	-0.6	1878	0.7	4717	44
1090	203	14	1251	279	760	-0.12	-0.642	1928	0.734	2070	44
1141	216	57	771	223	457	-0.097	-0.464	1168	0.257	18,548	44
1141	227	59	925	277	814	-0.066	-0.514	1127	0.309	5053	44
1141	220	53	695	199	418	-0.096	-0.462	1117	0.264	24,402	44
A538Aa	185	67	1515	405	1482	-0.065	-0.62	1655	0.3	280	47
A538Ba	185	56	1860	460	1793	-0.071	-0.71	2135	0.8	380	47
1541F	206	49	951	290	889	-0.076	-0.65	1276	0.68	1794	47
1541F	206	60	889	260	786	-0.071	-0.65	1276	0.93	2871	47
A538Ca	180	55	200	480	1931	-0.07	-0.75	2240	0.6	149	47
AM-350b	180	20	1905	496	1861	-0.102	-0.42	2690	0.1	197	47
H-11	205	33	2585	660	2034	-0.077	-0.74	3170	0.08	6	47
RQC-100b	205	43	940	290	896	-0.07	-0.69	1240	0.66	968	47
RQC-100b	205	67	930	290	883	-0.07	-0.69	1240	0.66	968	47
10B62	195	38	1640	430	1510	-0.067	-0.56	1780	0.32	680	47
1005-1009	205	73	360	90	269	-0.09	-0.43	580	0.15	58,991	47
1005-1009	205	66	470	125	448	-0.059	-0.51	515	0.3	20,158	47
1005-1009	200	64	415	125	400	-0.073	-0.41	540	0.11	29,957	47
1005-1009	200	80	345	90	262	-0.109	-0.39	640	0.1	104,405	47
1015	205	68	415	80	228	-0.11	-0.64	825	0.95	15,010	47
1020	205	62	440	108	262	-0.12	-0.51	895	0.41	57,176	47
1040	200	60	620	225	345	-0.14	-0.57	1540	0.61	13,028	47
1045	200	65	725	225	634	-0.095	-0.66	1225	1	4127	47
1045	200	51	1450	410	1365	-0.073	-0.7	1860	0.6	385	47
1045	205	59	1345	390	1276	-0.074	-0.68	1585	0.45	409	47
1045	205	55	1585	450	1517	-0.07	-0.69	1795	0.35	192	47
1045	205	51	1825	500	1689	-0.08	-0.68	2275	0.25	90	47
1045	205	41	2240	595	1862	-0.081	-0.6	2725	0.07	12	47

(Continues)

TABLE A1 (Continued)

Steel type	E (GPa)	RA (%)	σ_u (MPa)	BHN (kgf/mm ²)	σ_y (MPa)	b	c	σ'_f (MPa)	ϵ'_f	N_f (cycles)	Ref.
4130	220	67	895	258	779	-0.083	-0.63	1275	0.92	5275	47
4130	200	55	1425	365	1358	-0.081	-0.69	1695	0.89	1042	47
4142	200	29	1060	310	1048	-0.1	-0.51	1450	0.22	2060	47
4142	205	48	1415	380	1379	-0.08	-0.75	1825	0.45	175	47
4142	200	42	1760	450	1586	-0.08	-0.73	2000	0.4	146	47
4142	200	37	1930	450	1862	-0.09	-0.76	2105	0.6	209	47
4142	205	35	1930	475	1724	-0.081	-0.61	2170	0.09	29	47
4142	205	27	2240	560	1689	-0.089	-0.76	2655	0.07	6	47
4142	200	47	1550	400	1448	-0.09	-0.75	1895	0.5	204	47
4142	200	20	2035	475	1896	-0.082	-0.77	2070	0.2	37	47
4340	195	43	825	243	634	-0.095	-0.54	1200	0.45	7725	47
4340	200	38	1470	409	1372	-0.091	-0.6	2000	0.48	1005	47
4340	195	57	1240	350	1172	-0.076	-0.62	1655	0.73	1799	47
5160	195	42	1670	430	1531	-0.071	-0.57	1930	0.4	829	47
52,100	205	11	2015	518	1924	-0.09	-0.56	2585	0.18	143	47
9262	205	14	925	260	455	-0.071	-0.47	1040	0.16	2854	47
9262	195	33	1000	280	786	-0.073	-0.6	1220	0.41	1399	47
9262	200	32	1565	410	1379	-0.057	-0.65	1855	0.38	262	47
950C	205	69	565	150	324	-0.11	-0.59	970	0.85	24,868	47
950X	205	65	440	150	345	-0.075	-0.54	625	0.35	13,457	47
950X	205	72	530	156	331	-0.1	-0.61	1005	0.85	12,279	47
980X	195	68	695	225	565	-0.08	-0.53	1055	0.21	1699	47
1144	195	33	930	265	717	-0.08	-0.58	1000	0.32	1947	47
1144	200	25	1035	305	1020	-0.09	-0.53	1585	0.27	1519	47
950C	205	64	565	159	315	-0.12	-0.61	1170	0.95	17,069	47
SNCM630	196	49	1100	327	951	-0.073	-0.823	1270	1.54	736	48
SNCM439	208	37	1050	323	950	-0.072	-0.801	1380	1.89	1164	48
525C	209	52	508	153	280	-0.096	-0.458	821	0.216	32,086	48
545C	206	39	798	234	590	-0.107	-0.561	1400	0.449	5102	48
SFNCM85S	201	66	825	241	565	-0.092	-0.522	1040	0.316	7114	48
SF60	208	53	820	167	580	-0.082	-0.439	978	0.187	15,120	48
SCM435	210	66	951	300	795	-0.067	-0.708	1100	0.996	1797	48
SCM440	204	36	1000	319	846	-0.088	-0.65	1400	0.675	1757	48